Journal of Environmental Chemical Engineering 8 (2020) 103740

Contents lists available at ScienceDirect

Journal of Environmental Chemical Engineering

journal homepage: www.elsevier.com/locate/jece

Enhancement of CO_2/N_2 selectivity and CO_2 uptake by tuning concentration and chemical structure of imidazolium-based ILs immobilized in mesoporous silica

Rafael Duczinski[a], Barbara B. Polesso[a], Franciele L. Bernard[b], Henrique Z. Ferrari[b], Pedro L. Almeida[d,e], Marta C. Corvo[d], Eurico J. Cabrita[f], Sonia Menezes[c], Sandra Einloft[a,b,*]

[a] School of Technology, Pontifical Catholic University of Rio Grande do Sul – PUCRS, Av. Ipiranga, 6681, Building 30 – room 101.08, 90619-900, Porto Alegre, Brazil
[b] Post-Graduation Program in Materials Engineering and Technology – Pontifical Catholic University of Rio Grande do Sul – PUCRS, Brazil
[c] CENPES/PETROBRAS, sdu, Brazil
[d] CENIMATi3N, Materials Science Dep., School of Science and Technology, NOVA University Lisbon, Portugal
[e] ISEL, ADF, Lisbon, Portugal
[f] UCIBIO, Chemistry Dep. School of Science and Technology, NOVA University Lisbon, Portugal

ARTICLE INFO

Keywords:
Immobilization
Ionic liquids
CO_2capture

ABSTRACT

Imidazolium-based ionic liquids (ILs) with different cation alkyl chain ([*i*-C_5mim] or [C_4mim]) and inorganic anions ([Cl^-], [Tf_2N^-], [PF_6^-] and [DCA^-]) were synthesized and immobilized in commercial mesoporous silica. The synthesized supported ILs (SILs) were characterized using NMR, FTIR, TGA, BET, SEM and TEM. CO_2 sorption capacity, reusability and CO_2/N_2 selectivity were assessed by the pressure-decay technique. The effects of IL concentration, cation and anion chemical structure in CO_2 sorption capacity and CO_2/N_2 separation performance were evaluated. Tests evidenced that the presence of branching on the cation alkyl side chain increases CO_2/N_2 selectivity. The immobilization of the IL [*i*-C_5TPIm][Cl] on mesoporous silica in different concentrations (50, 20, 10 and 5 %) revealed that lower IL concentration results in higher CO_2 sorption capacity. Immobilization of ILs containing fluorinated anions at low concentrations in the mesoporous silica support may promote the improvement of the CO_2/N_2 selectivity without interfering on CO_2 sorption capacity of the original support. CO_2 sorption capacity value shown by sample SIL-5 % - [*i*-C_5TPIm][Tf_2N] (79.50 ± 0.70 mg CO_2 g^{-1}) was close to the value obtained for the pristine mesoporous silica (81.70 ± 2.20 mg CO_2 g^{-1}) and the selectivity (4.30 ± 0.70) was more than twice of the one obtained for the support alone (2.32 ± 0.4). Recycle tests demonstrated that the ILs immobilized in mesoporous silica samples are stable, providing a new option to be used in CO_2 capture processes.

1. Introduction

A large amount of greenhouse gases (GHG) needs to be reduced to mitigate the climate change effect. Carbon dioxide (CO_2) has been confirmed as the main greenhouse gas deriving from human activity [1–3]. Carbon capture and storage (CCS) is considered a crucial strategy for climate change mitigation efforts. Several technologies have been proposed to separate CO_2 from combustion exhaust gases. CO_2 chemical absorption process using aqueous amine solutions is the most mature technology [1,4–6], but it is costly and particularly harmful to the environment due to high equipment corrosion rate, large energy penalty for solvent regeneration and amine degradation/evaporation [1,7–9].

Room-temperature ionic liquids (RTILs) are salts composed of organic cations and organic or inorganic anions with a melting point lower than 100 °C [10,11]. RTILs are alternative solvents for CO_2 capture because they exhibit unique properties like high thermal stability, non-flammability, negligible vapor pressure, tenability and selective CO_2 absorption in gas mixtures [1,11,12]. However, RTILs high price and viscosity can represent a barrier to implementation in the oil and gas industry [11]. More recently, supported ILs (SILs) have been gathering attention as an option to high viscosity RTILs and are nowadays considered promising sorbents for CO_2 capture. SILs are generally prepared by chemical immobilization techniques through

* Corresponding author at: Post-Graduation Program in Materials Engineering and Technology – Pontifical Catholic University of Rio Grande do Sul – PUCRS, Brazil.
E-mail address: einloft@pucrs.br (S. Einloft).

https://doi.org/10.1016/j.jece.2020.103740
Received 26 November 2019; Received in revised form 22 January 2020; Accepted 1 February 2020
Available online 03 February 2020
2213-3437/ © 2020 Elsevier Ltd. All rights reserved.

covalent bonds or physical immobilization [13]. SILs present reversible CO_2 sorption/desorption performance with very fast kinetics compared to RTILs. These characteristics make CO_2 capture with SILs an attractive and environmentally friendly process. RTILs based on alkyl-imidazolium cations are the most commonly investigated for CO_2 capture applications [14–19]. Different types of adsorbent materials including cellulose [20,21], activated carbon [22–25], zeolites, carbon molecular sieves and mesoporous silica [26] have been explored as immobilization materials for IL species. Polyethyleneimine and the IL [Emim][Ac] were physically immobilized on SBA-15 silica support. The IL was added to work as an additive aiming to optimize the CO_2 sorption performance of the immobilized amine [27]. Nevertheless, CO_2 selectivity data (CO_2/N_2) in flue gases is, to date, still very scarce in the literature. Among silica-based materials, mesoporous silicas have attracted significant research interest for CO_2 adsorption due to their high specific surface area, uniform and tunable large pore sizes, and functional surface groups [28].

In this work, we have prepared several imidazolium-based SILs by chemical immobilization technique in mesoporous silica and studied the effect of IL concentration, alkyl chain branching in the imidazolium cation (1-isopentyl-3-methylimidazolium [*i*-C_5mim] or 1-butyl-3-methylimidazolium [C_4mim]) and inorganic anions (chloride [Cl^-], bis (trifluoromethylsulfonyl)imide [Tf_2N^-], hexafluorophosphate [PF_6^-] and dicyanamide [DCA^-]) on CO_2/N_2 selectivity.

2. Materials and methods

Mesoporous silica was donated by Petróleo Brasileiro S. A. (PETROBRAS). Imidazole (99 % Sigma Aldrich), (3-chloropropyl)-triethoxysilane (CPTES, 95 % Sigma Aldrich), 1-chlorobutane (99.5 % Sigma Aldrich), 1-bromo-3-methylbutane (96 % Sigma Aldrich), sodium hydride (NaH, 90 % Sigma Aldrich), tetrahydrofuran (THF, PA, Química Moderna), toluene (VETEC), ethyl ether (PA, Synth), chloroform-d (99.96 % with TMS, Sigma Aldrich), acetone (PA, VETEC), bis(trifluoromethane)sulfonimide lithium salt (99.95 %, Sigma Aldrich), sodium hexafluorophosphate (98 %, Sigma Aldrich) and sodium dicyanamide (96 %, Sigma Aldrich).

2.1. Ionic liquids synthesis

1-butyl-3-(triethoxysilylpropyl)imidazolium chloride [C_4TPIm][Cl] and 1-isopentyl-3-(triethoxysilylpropyl)imidazolium chloride [*i*-C_5TPIm][Cl] IL were synthesized following procedures adapted from literature [29–32]. Firstly, NaH was dissolved in THF. Then, imidazole in a 1:1 ratio (NaH : imidazole) was added to the solution and heated under reflux in N_2 atmosphere to form sodium imidazole. 1-chlorobutane or 1-bromo-3-methylbutane in a 1:1 ratio was added to the sodium imidazole and kept under stirring in N_2 atmosphere at 65 °C overnight. Afterwards, CPTES was added to the mixture and the system was stirred at 95 °C for 48 h. Yellowish and viscous ionic liquid with [Cl^-] anion ([C_4TPIm] [Cl] or [*i*-C_5TPIm] [Cl]) were obtained. [C_4TPIm][Cl], ^{1}H NMR (400 MHz, $CDCl_3$) δ ppm: 0.75 (t, 2 H), 0.95 (t, 3 H), 1.23 (t, 9 H), 1.37 (m, 2 H), 1.80 (m, 2 H), 1.91 (m, 2 H), 3.82 (q, 6 H), 4.39 (t, 4 H), 7,02 (s, 1 H), 7.15 (s, 1 H), 10.78 (s, 1 H) and [*i*-C_5TPIm][Cl], ^{1}H NMR (400 MHz, $CDCl_3$) δ ppm: 0.75 (t, 2 H), 0.97 (d, 6 H), 1.21 (t, 9 H), 1.64 (m, 1 H), 1.82 (m, 2 H), 2.02 (m, 2 H), 3.82 (q, 6 H), 4.39 (t, 4 H), 7.02 (s, 1 H), 7.15 (s, 1 H), 10.64 (s, 1 H).

2.2. Mesoporous silica-grafted ionic liquids synthesis

SILs (Fig. 1) were prepared using experimental procedures adapted from literature [33,34]. ILs grafting in commercial mesoporous silica was carried out in different concentrations (5–50 wt%). The IL ([C_4TPIm] [Cl] or [*i*-C_5TPIm] [Cl]) was dissolved in toluene and mixed with silica in a glass reactor under N_2 atmosphere at 95 °C for 48 h. After the reaction, the unreacted reagents were removed by Soxhlet extraction using ethyl ether for 3 h. The [Cl^-] anion was exchanged for [Tf_2N^-], [PF_6^-] and [DCA^-] only on the support grafted with [i-C_5TPIm][Cl] IL, using procedures adapted from literature [32,35]. SILs were labeled as SIL-Z%-[Y] [X], where Z is IL theoretical concentration, Y is the cation and X is the anion, for example, SIL-20 %-[i-C_5TPIm] [Cl] means 20 %wt of IL, [i-C_5TPIm] cation and Cl anion.

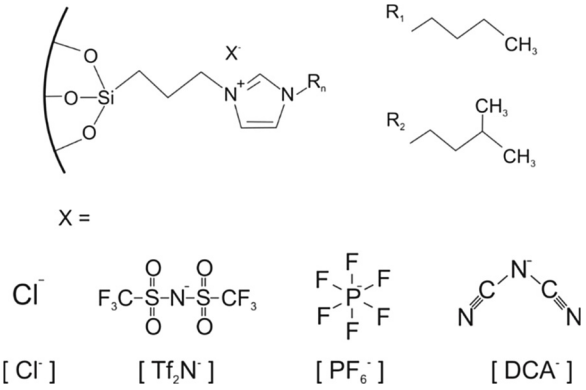

Fig. 1. Structure of IL supported on commercial mesoporous silica.

2.3. Characterization

The chemical composition of SILs samples were characterized by energy dispersion X-ray spectrometry (EDS), Field emission scanning electron microscopy (FESEM) was performed using a FEI Inspect F50 equipment in secondaryelectrons (SE) mode. The ^{1}H Nuclear Magnetic Resonance (NMR) spectra of ionic liquids were recorded before the immobilization on a Bruker Avance DRX-400 spectrometer operating at 400 MHz for ^{1}H and 100 MHz for ^{13}C. Solid state NMR (ssNMR) spectra were acquired with a 300 MHz AVANCE III Bruker spectrometer operating respectively at 300 MHz for ^{1}H, 75 MHz for ^{13}C and 60 MHz for ^{29}Si. SSNMR was performed using either a BBO probe head for magic angle spinning (MAS) analysis or a high-power wide line 5 mm probe head for static ^{1}H relaxation measurements. The MAS experiments were acquired spinning the sample at the magic angle at a frequency of 5 kHz in 4 mm-diameter rotors at room temperature. The ^{13}C MAS NMR experiments were acquired with proton cross-polarization (CPMAS) with a contact time of 1.2 ms, and the recycle delay was 2.0 s. The single pulse ^{29}Si MAS NMR experiments was acquired with a recycle delay of 10.0 s. The static ^{1}H NMR was acquired by accumulating 2 K data points over a spectral width of 250 kHz, using a 2.5 µs, 90° pulse with a recycle delay of 5 s between acquisitions. *T_1rho* measurements were performed using a spinlock of 10 kHz between 303 and 333 K. Textural properties were analyzed by nitrogen adsorption-desorption isotherm from NOVA 4200e High Speed at liquid nitrogen temperature. Surface area and pore size were determined by Brunauer-Emmett-Teller (BET) and Barrett-Joyner-Halenda (BJH) methods, respectively. Transmission electron microscopy (TEM) was used in the evaluation of the support structure. Samples were analyzed in Tecnai G2 T20 FEI operating at 200 KV.

Thermogravimetric Analysis (TGA/DTG) was performed using TA Instruments SDT-Q600 between 25 and 800 °C with a heating rate of 20 °C min^{-1} in air. The IL loading in silica support (denoted as IL%) was calculated from the TGA curve using the following Eq. (1):

$$IL\ (\%) = \frac{W_{150} - W_{800}}{W_{150}} X\ 100 - 3{,}4^{*} \quad (1)$$

Where, W_{150} and W_{800} are sample weight (g) at 150 °C and 800 °C, respectively and (*) is a correction factor related to second stage of weigh loss of pristine support.

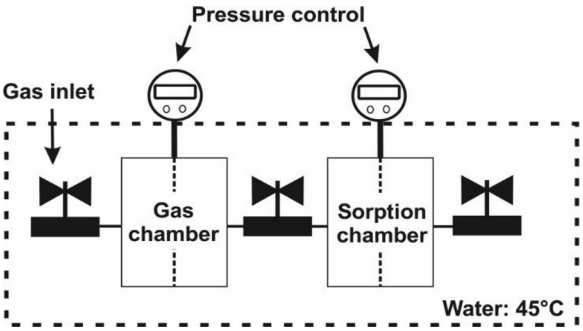

Fig. 2. Sorption cell.

2.4. Sorption experiments

2.4.1. CO_2 sorption measurements

The pressure-decay technique [36] for determining the CO_2 sorption capacity that has been previously reported by our group [21,26,37] was used. The experiments were carried out in triplicate in a gas sorption cell, Fig. 2. The samples (Ws ≈ 1 g) were previously degassed at 70 °C for 2 h. CO_2 sorption measurements were carried out at 45 °C (318.15 K) and 0.4 MPa. The CO_2 sorption capacity ($w_{CO_2/g}$) was calculated using equations (2) and (3).

$$n_{CO_2} = \frac{p_i V_{gc}}{Z_{(Pi,\,Ti)} R T_i} - \frac{p_{eq}(V_t - V_s)}{Z_{(p_{eq},T_{eq})} R T_{eq}} \quad (2)$$

$$w_{CO_2/g} = \frac{n_{CO_2} M}{W_s} \quad (3)$$

where n is the number of mols, p_i and T_i are the pressure and temperature in the gas chamber, V_{gc} is the volume of gas chamber, p_{eq} and T_{eq} are the pressure and temperature at equilibrium in the sorption chamber, V_s is the volume of the sample, V_t is the total volume of the sorption chamber, Z is compressibility factor for the pure gas calculated by the Span-Wagner equations-of-state for CO_2 [38].

2.4.2. Sorption/desorption tests

Sorption/desorption tests used CO_2. Three CO_2 sorption/desorption cycles were performed in SIL sample. CO_2 sorption was evaluated at 45 °C (318.15 K) and 0.4 MPa with desorption following each cycle using heating (343.15 K) during 2 h.

2.4.3. CO_2/N_2 separation selectivity

The selectivity experiments were carried out at 45 °C and 2 MPa using in a dual-chamber gas sorption cell similar to Koros et al. (Fig. 2) [36]. The samples (Ws ≈ 1 g) were also previously degassed at 70 °C for 2 h. The CO_2/N_2 selectivity experiments were conducted using a binary mixture (15.89 mol % of CO_2 and N_2 balance). A detailed description of the sorption apparatus and measuring procedure can be found in previous works [26,39,40]. CO_2 selectivity over N_2 was calculated using equation (4)

$$S = \frac{X_{CO_2}/Y_{CO_2}}{X_{N_2}/Y_{N_2}} \quad (4)$$

Where X_{CO_2} and X_{N_2} are molar fractions of CO_2 and N_2 in sample phase and Y_{CO_2} and Y_{N_2} are molar fractions of CO_2 and N_2 in gas phase, respectively

3. Results and discussion

The grafting of imidazolium ILs on the mesoporous silica was studied by ^{29}Si MAS NMR spectroscopy (Fig. 3). Mesoporous silica presents three resonances at –112, –104 and –93 ppm, assigned to the $[Si(OSi)_4]$ (Q^4), $[Si(OSi)_3OH]$ (Q^3) and $[Si(OSi)_2(OH)_2]$ (Q^2) species on the silica framework, respectively. Comparing the relative intensities of Q bands before and after grafting, it is possible to see variations in the Q^4/Q^3 ratio, especially in samples SIL-5 %-[*i*-C_5TPIm][DCA] and SIL-5 %-[*i*-C_5TPIm][PF_6], where the reduction of Q^3 and Q^2 bands, and relative increase of the Q4 peak is more obvious. These changes suggest that the hydroxyl groups in silica have reacted and that the IL molecules were successfully anchored.

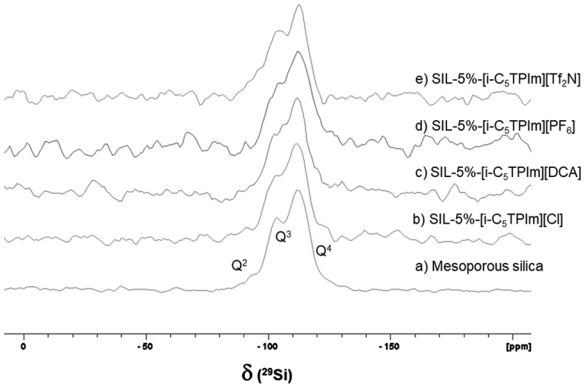

Fig. 3. Solid state ^{29}Si MAS NMR spectra of mesoporous silica (a); SIL-5 %-[i-C_5TPIm][Cl] (b); SIL-5 %-[i-C_5TPIm][DCA] (c); SIL-5 %-[i-C_5TPIm][PF_6] (d) and SIL-5 %-[i-C_5TPIm][Tf_2N] (e).

To reinforce the conclusions from ^{29}Si NMR analysis, SILs with a higher IL content were further analyzed (Fig. 4).

Both ^{13}C CP-MAS NMR and ^{29}Si MAS NMR analyses confirm the modification of the mesoporous silica. In ^{13}C spectra, imidazolium ring resonance appears between 108 and 140 ppm, and the aliphatic signals between 60 and 5 ppm. The ^{29}Si NMR spectra display not only Q^3 and Q^4 bands, but also T^2 and T^3 signals at - 60 and - 70 ppm, characteristic of $[RSi(OSi)_2(OMe)]$ and $[RSi(OSi)_3]$ moieties, respectively.

However, the certainty of the successful grafting of SILs does not provide further evidence on how the different IL moieties exist in the silica matrix. In an attempt to gather additional information, a NMR relaxation study was performed. In particular, rotating-frame relaxation measurements (T_1rho), can be used to probe intermolecular interactions, particles dispersion and distribution [41]. In Fig. 5, the T_1rho for SIL-5 %-[*i*-C_5TPIm][X] from different IL anions and SIL- [i-C_5TPIm][Tf_2N] with different IL contents can be observed. All samples exhibited a biexponential behavior, which is compatible with the existence of a more restrained proton population, with a $T_1rho < 0.01$ s, due to the silica matrix itself, and a more mobile, with a longer T_1rho, influenced by the IL moiety. This behavior is known in silica matrixes due to their porous nature. Proton moieties that reside near the surface layer exhibit faster relaxation because of the interactions with the pore wall, and proton moieties that reside in a bulk-like layer in the middle of pores, the relaxation times are longer because bulk diffusion processes may dominate [42].

From the comparison of the data for the 5 % SILs samples with different anions, it is possible to conclude that smaller and more hydrophilic anions, such as chloride, have a more restrained behavior (lower T_1rho) than the rest, while the DCA SIL exhibits a population with a higher degree of freedom. The effect of increasing the amount of IL can be observed for SIL-X%-[*i*-C_5TPIm][Tf_2N] and suggests that an amount of IL as 50 % will be less mobile than lower amounts, which is compatible, in this case, with the IL being located inside and outside the matrix porous. In SILs with a lower IL content, the IL location is less restrained, and can in principle be more available to interact.

Chemical composition of [*i*-C_5TPIm][Cl] SILs samples were analised by EDS before and after anion exchange (Fig. 6). Characteristic elements of each anion ($[Cl^-]$, $[Tf_2N^-]$, $[PF_6^-]$ or $[DCA^-]$) were detected by EDS. The appearance of new peaks and the absence of $[Cl^-]$ anion in the samples SIL-5 %-[i-C_5TPIm][Tf_2N], SIL-5 %-[i-C_5TPIm][PF_6] and

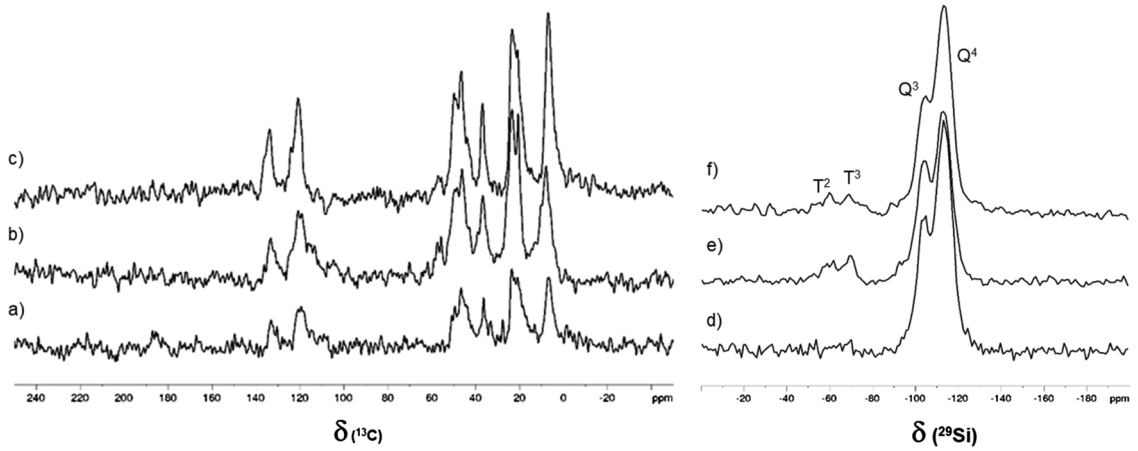

Fig. 4. Solid state ^{13}C CP-MAS and ^{29}Si MAS NMR spectra of SIL-10 %-[i-C_5TPIm][Tf_2N] (a,d); SIL-20 %-[i-C_5TPIm][Tf_2N] (b,e); SIL-50 %-[i-C_5TPIm][Tf_2N] (c,f).

SIL-5 %-[i-C_5TPIm][DCA] indicates effective anions exchange.

Fig. 7 shows TEM images of the mesoporous silica used as a support before and after IL immobilization. Mesoporous silica (Fig. 7a) presents regions where it is possible to identify the silica lamellar structure. After IL immobilization this lamellar structure is no longer identified (see Fig. 7b). This change can be attributed to IL immobilization on silica. Fig. 7b shows a typical image of the mesoporous silica structure after IL immobilization.

Textural properties and immobilized IL (%) concentration in samples are shown in Table 1. The textural properties of mesoporous silica are modified after IL immobilization. Specific surface area reduction is related to immobilized IL concentration as seen in Table 1. Higher immobilized IL concentrations promote greater specific surface area reduction. Compare sample SIL-50 %-[i-C_5TPIm][Cl] presenting a specific surface area of 186 $m^2\ g^{-1}$, with pristine mesoporous silica sample exhibiting specific surface area of 487 $m^2\ g^{-1}$. Pore volume follows a similar behavior to that seen for the specific surface area. The pore volume of sample SIL-50 %-[*i*-C_5TPIm][Cl] (0.27 cm^3) is 64 % lower when compared to the support pore volume before immobilization (0.75 cm^3). This difference decreases depending on the IL immobilized content (see Table 1).

Table 2 presents textural properties data for supported samples with 5 % IL. The specific surface area of sample SIL-5 %-[i-C_5TPIm][PF_6] (380 $m^2\ g^{-1}$) is lower when compared to sample SIL-5 %-[i-C_5TPIm][Tf_2N] (426 $m^2\ g^{-1}$) and SIL-5 %-[i-C_5TPIm][DCA] (414 $m^2\ g^{-1}$).

Pore volume of all samples tends to decrease with the increasing amount of immobilized IL independent of anion type ([Cl^-], [Tf_2N^-], [PF_6^-] and [DCA^-]) as seen in Table 1 and 2. The reduction of support specific surface area is a consequence of increasing immobilized IL content [30,43] as shown in Tables 1 and 2. Samples SIL-5 %-[i-C_5TPIm][Cl] (355 $m^2\ g^{-1}$) and SIL-5 %-[*i*-C_5TPIm][Tf_2N] (426 $m^2\ g^{-1}$) presented higher specific surface area values when compared to samples SIL-50 %-[*i*-C_5TPIm][Cl] (186 $m^2\ g^{-1}$) and SIL-50 %-[*i*-C_5TPIm][Tf_2N] (157 $m^2\ g^{-1}$) respectively, probably due to the lower immobilized IL content. Fig. 8 shows the N_2 adsorption/desorption isotherms of mesoporous silica support and immobilized IL mesoporous silica samples. The curves height in the N_2 adsorption/desorption isotherms depends on the textural properties of each sample. Looking at Table 1 and Fig. 8(II) for samples SIL-X%-[i-C_5TPIm][Cl] one can see that specific surface area (S_{BET}) and pore volume (V_p) for samples with 50 % and 20 % of IL are similar as well the curves height. However, the same behavior is not observed in Fig. 8(III). See that S_{BET} and V_p values for sample SIL-20 %-[i-C_5TPIm][Tf_2N] are ~80 % and ~130 % higher respectively when compared to sample SIL-50 %-[i-C_5TPIm][Tf_2N], meaning more space and volume to N_2 adsorption. Mesoporous silica samples, before and after ILs immobilization, presented type IV isotherm with hysteresis H1 characteristic of mesoporous solids [44,45], indicating that the presence of ILs showed no effect on the support mesoporous nature.

Thermal stability of mesoporous support before and after ILs chemical immobilization was evaluated (Fig. 9). Pristine mesoporous silica (Fig. 9a) shows two mass loss stages, the first one referring to water

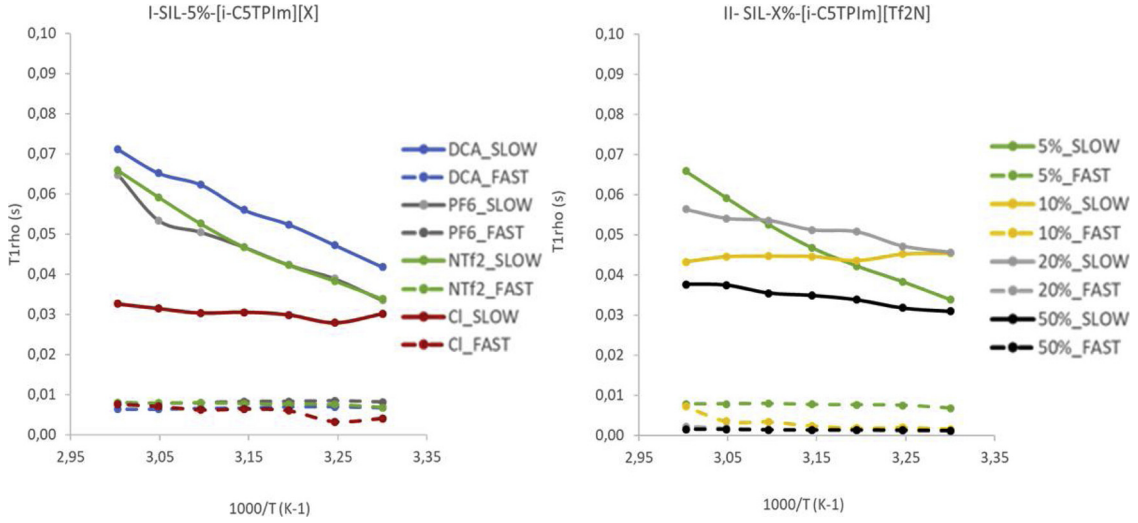

Fig. 5. ^1H T_1rho of SIL-5 %-[i-CTPIm][X] (I) and SIL-X%-[i-CTPIm][Tf_2N] (II).

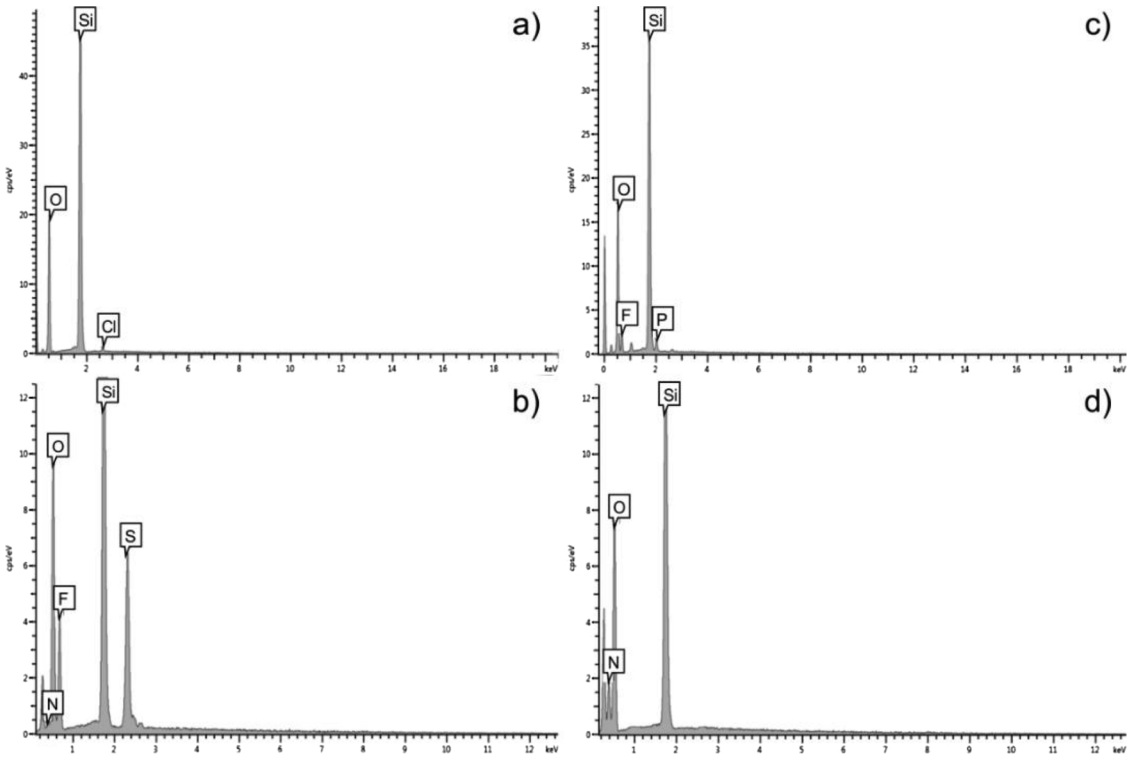

Fig. 6. EDS analysis from SILs before and after anion change: a) SIL-5 %-[i-C_5TPIm][Cl], b) SIL-5 %-[i-C_5TPIm][Tf_2N], c) SIL-5 %-[i-C_5TPIm][PF] and d) SIL-5 %-[i-C_5TPIm][DCA].

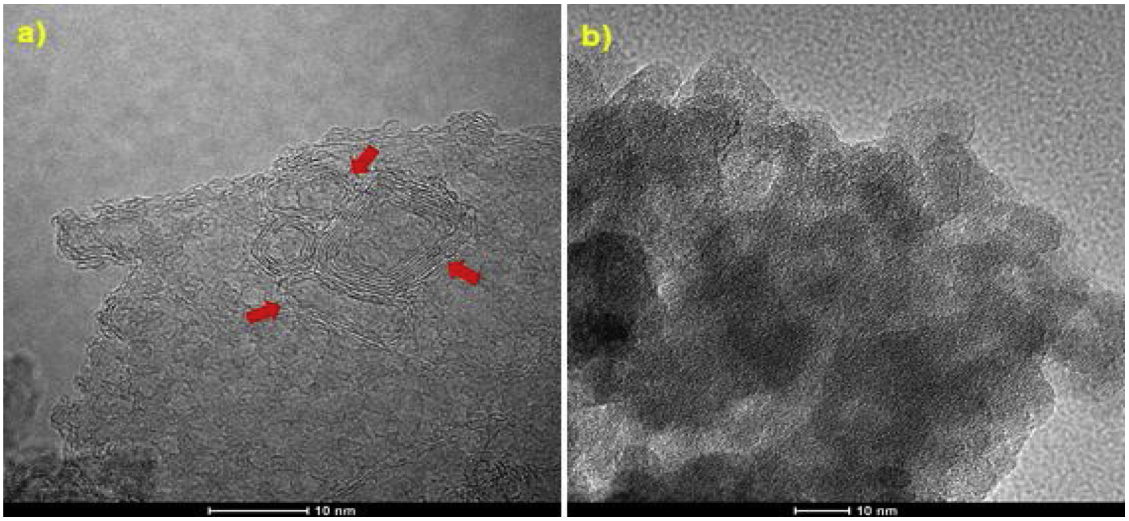

Fig. 7. TEM images: a) mesoporous silica, b) SIL-10 %-[i-C_5TPIm][Tf_2N].

superficially adsorbed (T_{onset} = 48 °C) and the second stage related to water present in the silica network (T_{onset} 262 °C) [46]. After IL immobilization four thermal events are observed in all samples. The first mass loss stage with T_{onset} around 150 °C is attributed to moisture, the second one around 280 °C (T_{onset}) is related to IL organic fraction degradation, the third stage around 400 °C (T_{onset}) is associated with the anion degradation and the fourth stage above 400 °C (T_{onset}) attributed to silane groups bonded to silica support degradation [47,48]. The exchange of [Cl^-] anion by [Tf_2N^-], [DCA^-] or [PF_6^-] anions (Fig. 9c,d) maintain almost constant the samples thermal stability. However, small variations in the mass loss percentage of the third stage were observed. This behavior also evidences the successful exchange of [Cl^-] anion by the anions [Tf_2N^-], [DCA^-] or [PF_6^-]. IL immobilization increased residue percentage due to the organic fraction.

3.1. Cation's influence on CO_2 uptake and CO_2/N_2 selectivity of ILs immobilized mesoporous silica

Changes in IL cation structure such as alkyl side chain size or branching can modify ILs CO_2 solubility as reported in the literature [49–54]. In this work, the ILs [C_4TPIm][Cl] and [*i*-C_5TPIm][Cl] were selected for the evaluation of imidazolium cation alkyl chain effect on SILs CO_2 affinity and selectivity. CO_2 sorption capacity and CO_2/N_2 selectivity of SILs (SIL-15 %-[C_4TPIm][Cl] and SIL-15 %-[i-C_5TPIm][Cl]) compared to pristine mesoporous silica are presented in Table 3.

As seen in Table 3, CO_2 sorption capacity of sample SIL-15 %-[*i*-C_5TPIm][Cl] (66.20 ± 0.35 mg $CO_2\,g^{-1}$) was slightly higher when compared to sample SIL-15 %-[C_4TPIm][Cl] (63.70 ± 1.47 mg $CO_2\,g^{-1}$). However, in both cases, the CO_2 sorption capacity of the

Table 1
Textural properties and IL concentration (%) immobilized on the samples.

Sample	% (IL)**	S_{BET} ($m^2 g^{-1}$)	V_p (cm^3)	P_s (nm)
Sílica	–	487	0.75	2.69
SIL-15 %-[C_4TPIm][Cl]	13.18 ± 0.25	341	0.49	2.38
SIL-15 %-[i-C_5TPIm][Cl]	11.02 ± 0.48	365	0.53	2.72
SIL-50 %-[i-C_5TPIm][Cl]	29.80 ± 1.60	186	0.27	2.38
SIL-20 %-[i-C_5TPIm][Cl]	16.90 ± 0.74	173	0.24	2.39
SIL-10 %-[i-C_5TPIm][Cl]	5.0 ± 0.30	462	0.68	2.72
SIL-5 %-[i-C_5TPIm][Cl]	3.68 ± 0.83	461	0.68	2.71
SIL-50 %-[i-C_5TPIm][Tf_2N]	26.40 ± 0.04	157	0.21	1.69
IL-20 %-[i-C_5TPIm][Tf_2N]	19.72 ± 0.96	283	0.49	2.90
SIL-10 %-[i-C_5TPIm][Tf_2N]	6.5 ± 0.90	414	0.64	2.72
SIL-5 %-[i-C_5TPIm][Tf_2N]	3.78 ± 1.10	426	0.62	2.15

*S_{BET}: surface area, V_p: pore volume, P_s: pore size. **Determined by TGA.

Table 2
Textural properties of SILs with different anions.

Sample	% (IL)**	S_{BET} ($m^2 g^{-1}$)	V_p (cm^3)	P_s (nm)
SIL-5 %-[i-C_5TPIm][Tf_2N]	3.78 ± 1.10	426	0.62	2.15
SIL-5 %-[i-C_5TPIm][PF_6]	3.30 ± 0.14	380	0.57	2.10
SIL-5 %-[i-C_5TPIm][DCA]	2.35 ± 0.1	414	0.61	2.11

*S_{BET}: surface area, V_p: pore volume, P_s: pore size. **Determined by TGA.

mesoporous silica (81.70 ± 2.20 mg $CO_2 g^{-1}$) decreased after IL immobilization. This behavior is probably associated with specific surface area and pore volume reduction after IL immobilization (see Table 1) [26,55]. The specific surface area (487 $m^2 g^{-1}$) and pore volume (0.75 cm^3) values of pure mesoporous silica were reduced after ILs immobilization. See, for example, sample SIL-15 %-[C_4TPIm][Cl] (specific surface area of 341 $m^2 g^{-1}$ and pore volume of 0.49 cm^3) and sample SIL-15 %-[*i*-C_5TPIm][Cl] (specific surface area of 365 $m^2 g^{-1}$ and pore volume of 0.53 cm^3). Unlike the specific surface area, the selectivity CO_2/N_2 is improved when ILs are immobilized in mesoporous silica. Yet, the alkyl side chain plays an important role in CO_2/N_2 selectivity. Compare the selectivity of mesoporous silica (2.32 ± 0.4) with the selectivity of samples SIL-15 %-[*i*-C_5TPIm][Cl] containing a methyl group branching in the IL cation alkyl side chain (4.45 ± 0.82) and SIL-15 %-[C_4TPIm][Cl] (2.68 ± 0.50) without ramification in the IL cation alkyl side chain. The presence of branching in the IL cation side alkyl chain promotes higher free space for CO_2 molecules [49,52]. The specific surface area and pore volume values obtained for samples SIL-15 %-[*i*-C_5TPIm][Cl] and SIL-15 %-[C_4TPIm][Cl] were similar (see Table 1) corroborating that the improvement in CO_2/N_2 selectivity for sample SIL-15 %-[*i*-C_5TPIm][Cl] may be related to the presence of cation alkyl side chain branching.

3.2. Influence of immobilized ILs concentration and anion type on mesoporous silica CO_2 uptake capacity and CO_2/N_2 selectivity

The concentration of ILs immobilized on silica supports plays a role in CO_2 uptake capacity as well as gas mixtures selectivity [26]. ILs [*i*-C_5TPIm][Cl] and [*i*-C_5TPIm][Tf_2N] were immobilized on mesoporous silica in different concentrations (50, 20, 10 and 5 %) in order to evaluate the influence in CO_2 uptake capacity as well as CO_2/N_2 selectivity. The immobilized IL concentration plays an important role in the sorption capacity since the excess of IL can reduce the porosity of the support or fill its pores [56]. The ideal IL concentration to be immobilized in support varies according to their composition, specific surface area and both pore size and volume [57,58]. [Tf_2N^-] anion was chosen for the tests due to its high affinity and selectivity for the CO_2

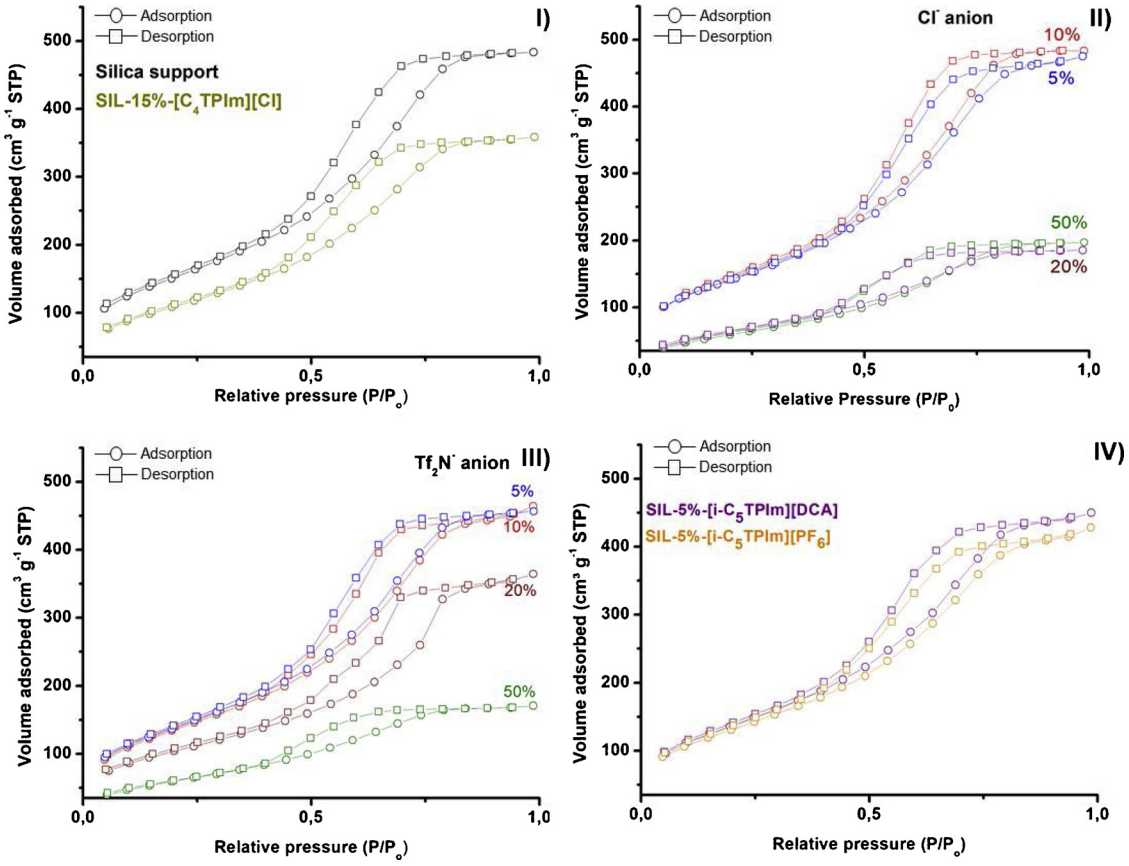

Fig. 8. N_2 adsorption/desorption isotherms. I) mesoporous silica and SIL-15 %- [C_4TPIm][Cl]; II) diferent concentrations of SIL- [i-C_5TPIm][Cl], III) diferent concentrations of [i-C_5TPIm][Tf_2N] and IV) 5 % concentration of [i-C_5TPIm] cations with [DCA] and [PF_6] anions.

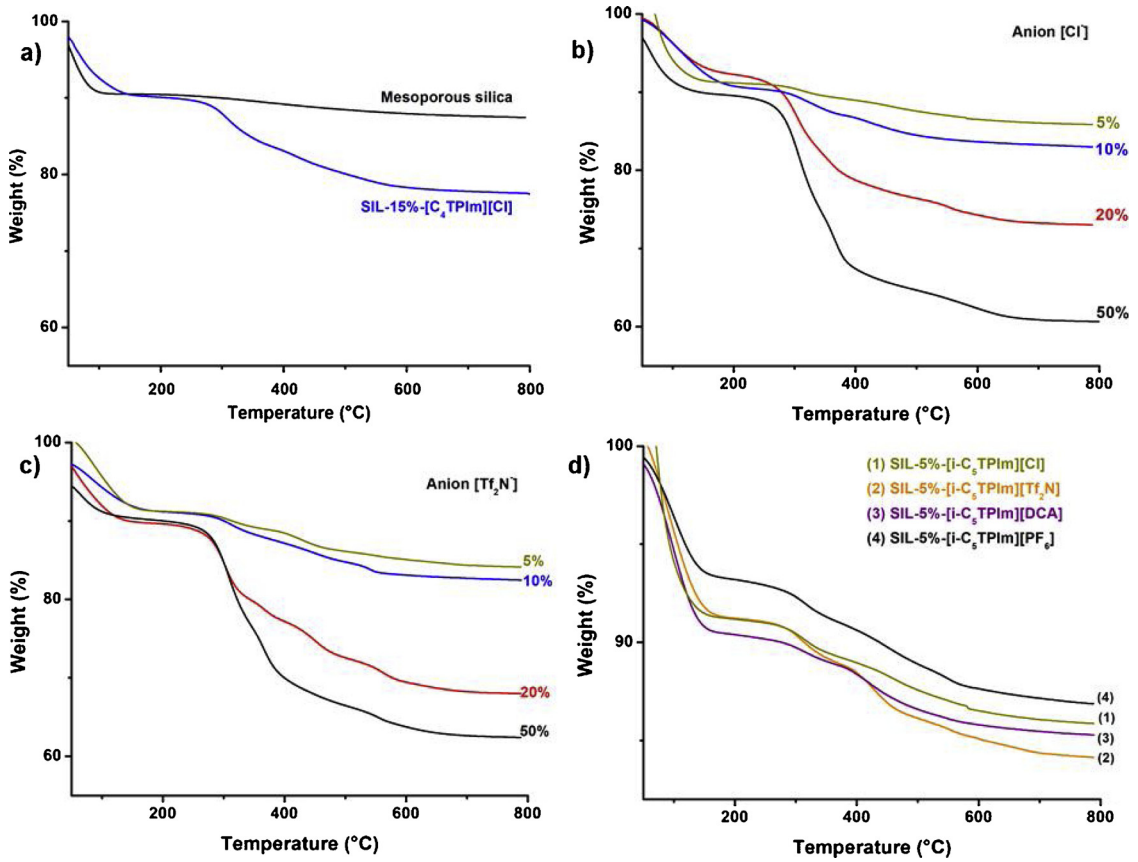

Fig. 9. SILs thermal stability : a) mesoporous silica and SIL-15 %-[C_4TPIm][Cl], b) diferent concentrations of [i-C_5TPIm][Cl], c) diferent concentrations of [i-C_5TPIm][Tf_2N] and d) SIL-5 %-[i-C_5TPIm] cation containing different anions.

Table 3
CO_2 sorption capacity and CO_2/N_2 selectivity of mesoporous silica and SILs samples.

Sample	CO_2 sorption (mg CO_2 g-1)	Selectivity CO_2/N_2
silica	81.70 ± 2.20	2.32 ± 0.40
SIL-15 %-[C_4TPIm][Cl]	63.70 ± 1.47	2.68 ± 0.50
SIL-15 %-[i-C_5TPIm][Cl]	66.20 ± 0.35	4.45 ± 0.82

molecule [59–61] in order to compare to [Cl^-] anion. After immobilization, the ILs molecules can be organized irregularly and first fill the support pores with a smaller size where the adsorption potential is higher [57]. As shown in Table 1, silica support specific surface area and pore volume decreased with increasing immobilized IL concentration. However, the type IV isotherm with hysteresis H1 characteristic of mesoporous solids was obtained for all samples (Fig. 8). The content of immobilized ILs and anion type changes samples CO_2 sorption capacity. Samples containing the [Cl^-] anion present lower CO_2 sorption capacity when compared to the pristine support (81.70 ± 2.20 mg CO_2 g^{-1}), the immobilization of larger amounts of ILs containing the [Cl^-] as anion, SIL-50 %-[*i*-C_5TPIm][Cl] (42.40 ± 0.70 mg CO_2 g^{-1}), decreases CO_2 sorption capacity in ~ 50 % when compared to pristine support. CO_2 sorption capacity is inverse to immobilized IL content. As can be observed for samples SIL-20 %-[*i*-C_5TPIm][Cl] (60.42 ± 0.35 mg CO_2. g^{-1}); SIL-10 %-[*i*-C_5TPIm][Cl] (60.63 ± 0.10 mg CO_2 g^{-1}) and SIL-5 %-[*i*-C_5TPIm][Cl] (67.50 ± 0.07 mg CO_2 g^{-1}).The best CO_2 sorption capacity was achieved for a sample containing 5 % of immobilized IL but yet lower when compared to the pristine support (81.70 ± 2.20 mg CO_2 g^{-1}). When [Tf_2N^-] is used as anion the same trend is observed but the CO_2 sorption capacity is superior when compared to results obtained when [Cl^-] is used as an anion (see Table 4). This behavior may

Table 4
Properties of SIL in different concentrations for [Cl^-] and [Tf_2N^-] anion.

Sample	CO_2 sorption (mg CO_2 g^{-1})	Selectivity CO_2/N_2
Silica	81.70 ± 2.20	2.32 ± 0.40
SIL-50 %-[i-C_5TPIm][Cl]	42.40 ± 0.70	4.82 ± 0.40
SIL-20 %-[i-C_5TPIm][Cl]	60.42 ± 0.35	3.20 ± 0.23
SIL-10 %-[i-C_5TPIm][Cl]	60.63 ± 0.10	4.34 ± 0.49
SIL-5 %-[i-C_5TPIm][Cl]	67.50 ± 0.07	3.80 ± 0.12
SIL-50 %-[i-C_5TPIm][Tf_2N]	63.86 ± 0.93	4.53 ± 0.50
SIL-20 %-[i-C_5TPIm][Tf_2N]	62.60 ± 1.00	4.34 ± 0.20
SIL-10 %-[i-C_5TPIm][Tf_2N]	69.38 ± 0.69	4.38 ± 0.24
SIL-5 %-[i-C_5TPIm][Tf_2N]	79.50 ± 0.70	4.30 ± 0.70

*S_{BET}: surface area, V_p: pore volume, P_s: pore size.

be associated with the affinity of [Tf_2N^-] anion by the CO_2 molecule [59–61]. The higher CO_2 sorption capacity achieved when [Tf_2N^-] was used as anion was obtained for sample SIL-5 %-[*i*-C_5TPIm][Tf_2N] (79.50 ± 0.70 mg CO_2 g^{-1}), similar when compared to pristine support. Immobilization of ILs in mesoporous silica improves CO_2/N_2 selectivity results for both anions when compared to pristine support. For immobilized ILs in concentrations of 50, 20 and 10 % the CO_2/N_2 selectivity is similar for both anions indicating that in high concentrations of IL there would be no benefits in the exchange of the [Cl^-] by [Tf_2N^-] (see Table 4). For IL concentration of 5 %, the sample SIL-5 % [*i*-C_5TPIm][Tf_2N] (4.30 ± 0.70) presents a slight difference when compared to sample SIL-5 %-[*i*-C_5TPIm][Cl] (3.80 ± 0.12). Comparing the selectivity of sample SIL-5 %-[*i*-C_5TPIm] [Tf_2N] with pristine mesoporous silica (2.32 ± 0.40) an increase in CO_2/N_2 selectivity of ~85 % was observed. The increase in CO_2/N_2 selectivity and the CO_2 sorption capacity value obtained for sample SIL-5 %-[*i*-C_5TPIm][Tf_2N] indicate that the IL immobilization in small percentages can promote a

selectivity improvement without compromising CO_2 sorption capacity. CO_2 sorption capacity and CO_2/N_2 selectivity of the SIL-5 %-[i-C5TPIm][Tf2N] sample are superior when compared to pristine silica support and similar to other samples described in literature under near CO_2 uptake tests conditions (P and T for sorption tests) but with higher IL content. The IL [P_{66614}] [Triz] was immobilized (50 %) in SBA-15 silica and its CO_2 sorption capacity and CO_2/N_2 selectivity evaluated at ~ 30 °C (29.7 mg CO_2 g^{-1} and 0.75 respectively) [62]. IL [P_{8883}] [TFSI] was immobilized (10 %) in commercial silica gel and the CO_2 sorption capacity at 40 °C and 4 bar of CO_2 pressure (70.4 mg CO_2 g^{-1}) and its CO_2/N_2 selectivity were evaluated increasing 100 % the selectivity comparing with pristine support [63]. The immobilization of a low percentage of ILs combined with the [Tf_2N^-] anion can be economically favorable, due to the high production cost of ionic liquids that often prevents its application on a large scale [57,64,65]. Improvement of CO_2/N_2 selectivity is essential for designing new materials to be used in CO_2 separation from exhaust gases [66,67].

3.3. Influence of imidazolium-based ILs with different anions [PF_6^-], [DCA^-], and [Tf_2N^-] immobilized on mesoporous silica supports in CO_2 uptake and CO_2/N_2 selectivity

The anion [Tf_2N^-] presented the best CO_2 sorption and selectivity results at the theoretical concentration of 5 % of immobilized IL. Anions [PF_6^-] and [DCA^-] in low concentration (5 %) will also be evaluated. Fluorinated anions such as [Tf_2N^-] and [PF_6^-] combined with solid supports present potential to improve CO_2 sorption capacity and selectivity as described in literature [68,69]. ILs having [DCA^-] as anion present lower viscosity values when compared to fluorinated anions [70]. This feature may facilitate the IL distribution over the support surface area. CO_2 sorption capacity for imidazolium ILs with these anions is reported in literature [70–73] in the following order [DCA^-] < [PF_6^-] < [Tf_2N^-]. Textural data of mesoporous silica support after immobilization with the three different ionic liquid are presented in Table 2. Pore size and pore volume values are similar for all samples. Specific surface area for sample SIL-5 %-[*i*-C_5TPIm][PF_6] (380 m^2g^{-1}) is lower when compared to samples SIL-5 %-[*i*-C_5TPIm][Tf_2N] (426 m^2g^{-1}) and SIL-5 %-[*i*-C_5TPIm][DCA] (414 m^2g^{-1}). The observed difference may be associated to the anion type. CO_2 sorption capacity and CO_2/N_2 selectivity at 45 °C are presented in Fig. 10. Sample SIL-5 %-[*i*-C_5TPIm] [DCA] presented CO_2 sorption capacity of 74.50 ± 0.70 mg CO_2 g^{-1}, superior to that shown when [Cl^-] was used as anion at the same IL concentration. The increase of CO_2 sorption capacity indicates the positive effect of the [DCA^-] anion on the CO_2 sorption capacity. However, the samples with fluorinated anions presented superior performance (SIL-5 %-[*i*-C_5TPIm][PF_6] (78.90 ± 1.50 mg CO_2 g^{-1}) and SIL-5 %-[*i*-C_5TPIm][Tf_2N] (79.50 ± 0.70 mg CO_2 g^{-1})). The specific surface area of sample SIL-5 %-[*i*-C_5TPIm][PF_6] (380 m^2 g^{-1}) was the smallest whereas samples SIL-5 %-[*i*-C_5TPIm][Tf_2N]) and SIL-5 %-[*i*-C_5TPIm][DCA] (414 m^2 g^{-1}) presented similar specific surface areas (Table 2). Nonetheles, all samples presented lower specific surface area values when compared to pristine mesoporous silica (487 m^2 g^{-1}). These results also indicate that although the SIL-5 %-[*i*-C_5TPIm] [PF_6] (380 m^2 g^{-1}) sample presented a lower specific surface area, the presence of [PF_6^-] anion compensated the reduction of the specific surface area due to the affinity of CO_2 with fluorinated anions [15,16,74,75]. CO_2 sorption capacity results were similar among the fluorinated anions ([PF_6^-] or [Tf_2N^-]) samples and the pristine mesoporous support. When CO_2/N_2 selectivity is evaluated the positive effect of anion exchange is seen in all samples regarding the selectivity of pristine mesoporous silica support (2.31 ± 0.40). The selectivity of samples SIL-5 %-[*i*-C_5TPIm] [Tf_2N] (4.3 ± 0.70), SIL-5 %-[*i*-C5TPIm][PF_6] (4.2 ± 0.20) and SIL-5 %-[*i*-C_5TPIm][DCA] (3.9 ± 0.30) are similar considering measurements deviation. Nevertheless, the CO_2 sorption capacity of fluorinated anion samples outperforms the [DCA^-] anion performance.

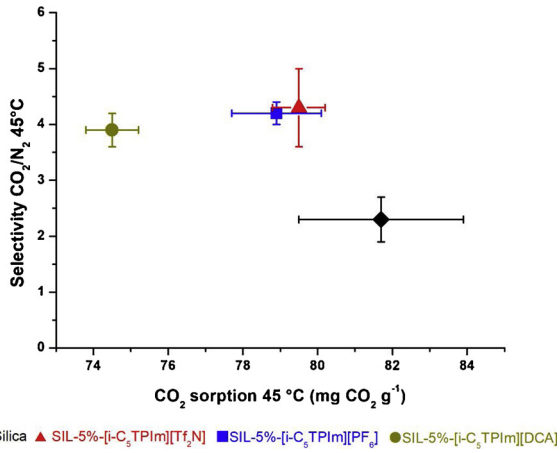

Fig. 10. CO_2 sorption and CO_2/N_2 selectivity of SIL-5 % - [i-C5TPIm] [x] samples with different anions.

Fig. 11 shows SEM images of mesoporous silica before and after ILs immobilization. Chemical immobilization of imidazolium-based ILs with different anions shows no changes in grain morphology observed on pure mesoporous silica. The low samples ILs content (Fig. 11 (b–e)) avoids grain agglomeration possibly contributing to sorption results observed for the samples.

Sorption/desorption tests were performed in order to evaluate the reusability of sample SIL-5 %-[*i*-C_5TPIm] [Tf_2N] at 45 °C and 0.4 MPa. Fig. 12 shows fives sorption/desorption tests using the same sample (SIL-5 % - [*i*-C_5TPIm] [Tf_2N]). Adsorbed CO_2 was removed by heating (~ 70 °C) at the end of each sorption test. Results showed that sample CO_2 sorption capacity is maintained between recycling steps indicating material stability.

4. Conclusions

ILs [C_4TPIm][Cl] and [*i*-C_5TPIm][Cl] chemical immobilization on mesoporous silica support were performed. Obtained materials were fully characterized to ensure the IL immobilization and determine their textural properties. CO_2 and CO_2/N_2 sorption test in different concentrations of IL [*i*-C_5TPIm][Cl] revealed that lower IL concentration results in higher CO_2 sorption capacity. Selectivity experiments with [C_4TPIm][Cl] and [*i*-C_5TPIm][Cl] evidenced that the presence of branching on the cation alkyl side chain increases CO_2/N_2 selectivity. Immobilization of ILs containing fluorinated anions ([PF_6^-] and [Tf_2N^-]) at low concentrations may also promote the improvement of the CO_2/N_2 selectivity without interfering with the CO_2 sorption capacity of the original support. CO_2 sorption capacity values shown by sample SIL-5 % - [*i*-C_5TPIm][Tf_2N] were close to the values obtained for the pristine mesoporous silica and their selectivity was more than twice when compared to the support. SIL-5 %-[*i*-C_5TPIm][PF_6] sample revealed similar CO_2 sorption capacity when compared to SIL-5 %-[*i*-C5TPIm][Tf_2N]. Sample SIL-5 %-[*i*-C_5TPIm][DCA] that presented a lower CO_2 sorption capacity. Finally, recycle tests demonstrated that the SILs in mesoporous silica samples are stable providing a new option to be used in CO_2 capture processes.

CRediT authorship contribution statement

Rafael Duczinski: Conceptualization, Methodology, Investigation. **Barbara B. Polesso:** Methodology, Investigation. **Franciele L. Bernard:** Conceptualization, Investigation, Methodology. **Henrique Z. Ferrari:** Investigation, Validation. **Pedro L. Almeida:** Conceptualization, Methodology, Investigation. **Marta C. Corvo:** Conceptualization, Methodology, Investigation. **Eurico J. Cabrita:** Conceptualization, Methodology, Investigation. **Sonia Menezes:** Conceptualization, Investigation, Project administration, Funding acquisition. **Sandra Einloft:** Conceptualization, Methodology, Project

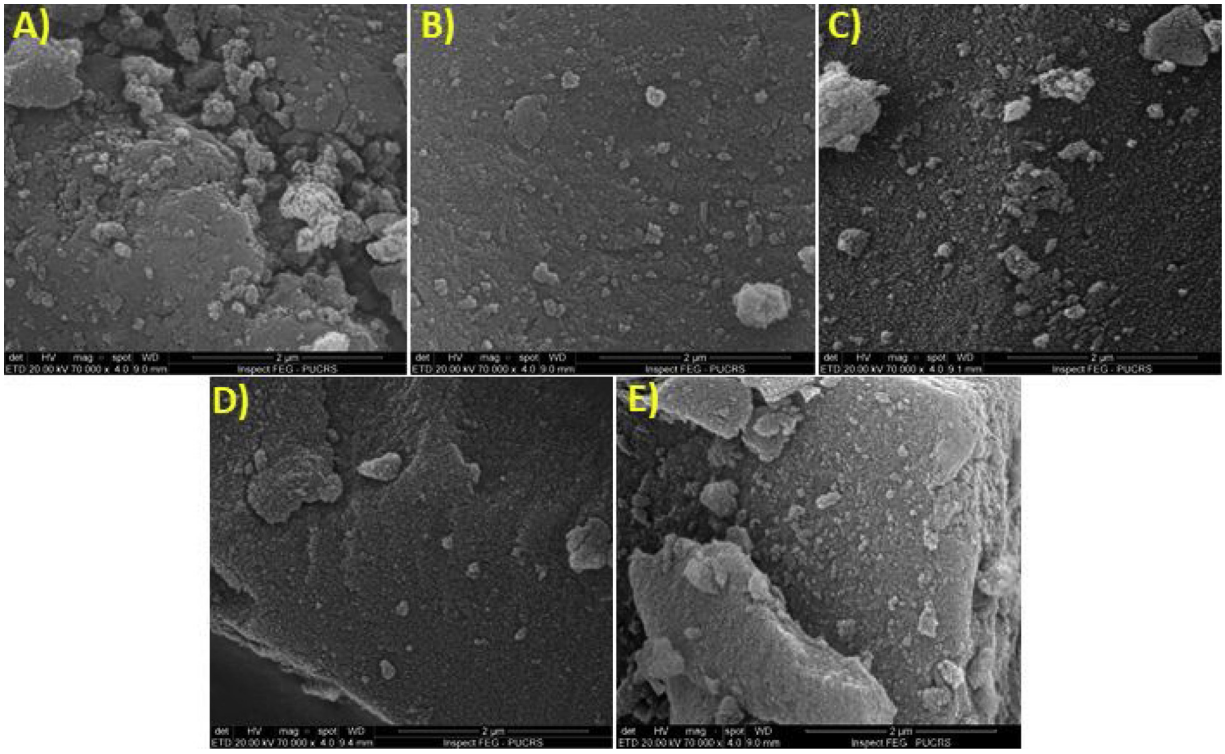

Fig. 11. SEM of samples: a) pristine mesoporous silica; b) SIL-5 %-[i-C_5TPIm][Cl]; c) SIL-5 %-[i-C_5TPIm][Tf_2N]; d) SIL-5 %-[i-C_5TPIm][PF_6] and e) SIL-5 %-[i-C_5TPIm][DCA].Magnification 70.000 x.

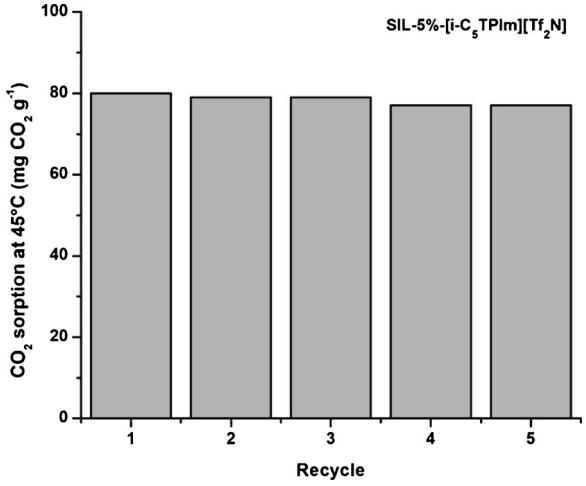

Fig. 12. CO_2 sorption capacity recycling tests at 45 °C and 0.4 MPa.

administration, Funding acquisition.

Declaration of Competing Interest

The authors declare that they have no known competing financial interests or personal relationships that could have appeared to influence the work reported in this paper.

Acknowledgments

Rafael Duczinski and Barbara B. Polesso thanks CAPES; Sandra Einloft thanks CNPq for research scholarship. This study was financed in part by the Coordenação de Aperfeiçoamento de Pessoal de Nível Superior – Brasil (CAPES) – Finance Code 001.This work was partially supported by Portuguese funding through FCT—Portuguese Foundation for Science and Technology, Portugal, under the projects PTDC/QUI-QFI/31508/2017, PORL, and PTNMR (ROTEIRO/0031/2013; PINFRA/22161/2016), co-financed by FEDER through COMPETE 2020, Portugal, POCI, and PORL and FCT through PIDDAC (POCI-01-0145-FEDER-007688; UID/CTM/50025/2019; and UID/Multi/04378/2019).

References

[1] A.U. Maheswari, K. Palanivelu, Carbon Dioxide Capture and Utilization by Alkanolamines in Deep Eutectic Solvent Medium, (2015), https://doi.org/10.1021/acs.iecr.5b01818.
[2] Z. Chen, C. Yang, Y. Chen, B. Yu, J. Wu, K. Shi, Y. Zhou, Spatiotemporal variations of CO2 emissions and their impact factors in China: a comparative analysis between the provincial and prefectural levels, Appl. Energy 233–234 (2018) 170–181, https://doi.org/10.1016/j.apenergy.2018.10.050.
[3] Y. Wang, C. Zheng, Y. Wang, H. Chen, Y. Xu, Thermodynamic validation of double bond comprised ionic liquids for CO2 capture, J. Environ. Chem. Eng. 7 (2019) 102774, , https://doi.org/10.1016/j.jece.2018.11.019.
[4] C. Dinca, N. Slavu, A. Badea, Benchmarking of the pre/post-combustion chemical absorption for the CO2 capture, J. Energy Inst. 91 (2018) 445–456, https://doi.org/10.1016/j.joei.2017.01.008.
[5] B. Aghel, E. Heidaryan, S. Sahraie, M. Nazari, Optimization of monoethanolamine for CO2 absorption in a microchannel reactor, J. CO2 Util. 28 (2018) 264–273, https://doi.org/10.1016/j.jcou.2018.10.005.
[6] W.H. Tay, K.K. Lau, A.M. Shariff, High frequency ultrasonic-assisted chemical absorption of CO2 using monoethanolamine (MEA), Sep. Purif. Technol. 183 (2017) 136–144, https://doi.org/10.1016/j.seppur.2017.03.068.
[7] T.E. Akinola, E. Oko, M. Wang, Study of CO2removal in natural gas process using mixture of ionic liquid and MEA through process simulation, Fuel 236 (2019) 135–146, https://doi.org/10.1016/j.fuel.2018.08.152.
[8] S. Hjelmaas, E. Storheim, N.E. Fløe, E.S. Thorjussen, A.K. Morken, L. Faramarzi, T. De Cazenove, E.S. Hamborg, Results from MEA amine plant corrosion processes at the CO2Technology centre mongstad, Energy Procedia 114 (2017) 1166–1178, https://doi.org/10.1016/j.egypro.2017.03.1280.
[9] A.A. Azmi, M.A.A. Aziz, Mesoporous adsorbent for CO 2 capture application under mild condition: a review, J. Environ. Chem. Eng. 7 (2019) 103022, , https://doi.org/10.1016/j.jece.2019.103022.
[10] S. Seo, L.D. Simoni, M. Ma, M.A. DeSilva, Y. Huang, M.A. Stadtherr, J.F. Brennecke, Phase-change ionic liquids for postcombustion CO2 capture, Energy Fuels 28 (2014) 5968–5977, https://doi.org/10.1021/ef501374x.
[11] M. Hasib-ur-Rahman, M. Siaj, F. Larachi, Ionic liquids for CO2 capture-Development and progress, Chem. Eng. Process. Process Intensif. 49 (2010) 313–322, https://doi.org/10.1016/j.cep.2010.03.008.

[12] W. Zhang, L. Ye, J. Jiang, CO2 capture with complex absorbent of ionic liquid, surfactant and water, J. Environ. Chem. Eng. 3 (2015) 227–232, https://doi.org/10.1016/j.jece.2014.07.020.
[13] L. Zhu, L. Guo, Z. Zhang, J. Chen, S. Zhang, The preparation of supported ionic liquids (SILs) and their application in rare metals separation, Sci. China Chem. 55 (2012) 1479–1487, https://doi.org/10.1007/s11426-012-4632-8.
[14] L.A. Blanchard, Z. Gu, J.F. Brennecke, High-pressure phase behavior of ionic liquid / {CO$_2$} systems, J. Phys. Chem. B 105 (2001) 2437–2444, https://doi.org/10.1021/jp003309d.
[15] J.L. Anthony, J.L. Anderson, E.J. Maginn, J.F. Brennecke, Anion effects on gas solubility in ionic liquids, J. Phys. Chem. B 109 (2005) 6366–6374, https://doi.org/10.1021/jp046404l.
[16] C. Cadena, J.L. Anthony, J.K. Shah, T.I. Morrow, J.F. Brennecke, E.J. Maginn, Why is CO2 so soluble in imidazolium-based ionic liquids? J. Am. Chem. Soc. 126 (2004) 5300–5308, https://doi.org/10.1021/ja039615x.
[17] E.I. Privalova, P. Mäki-Arvela, D.Y. Murzin, J.P. Mikkhola, Capturing CO 2 : conventional versus ionic-liquid based technologies, Russ. Chem. Rev. 81 (2012) 435–457, https://doi.org/10.1070/RC2012v081n05ABEH004288.
[18] J.L. Anthony, E.J. Maginn, J.F. Brennecke, Solubilities and thermodynamic properties of gases in the ionic liquid 1- n -Butyl-3-methylimidazolium hexafluorophosphate, J. Phys. Chem. B 106 (2002) 7315–7320, https://doi.org/10.1021/jp020631a.
[19] J.F. Brennecke, B.E. Gurkan, Ionic liquids for CO2 capture and emission reduction, J. Phys. Chem. Lett. 1 (2010) 3459–3464, https://doi.org/10.1021/jz1014828.
[20] F.L. Bernard, D.M. Rodrigues, B.B. Polesso, A.J. Donato, M. Seferin, V.V. Chaban, F.D. Vecchia, S. Einloft, New cellulose based ionic compounds as low-cost sorbents for CO2 capture, Fuel Process. Technol. 149 (2016) 131–138, https://doi.org/10.1016/j.fuproc.2016.04.014.
[21] F.L. Bernard, R.B. Duczinski, M.F. Rojas, M.C.C. Fialho, L.Á. Carreño, V.V. Chaban, F.D. Vecchia, S. Einloft, Cellulose based poly(ionic liquids): tuning cation-anion interaction to improve carbon dioxide sorption, Fuel 211 (2018) 76–86, https://doi.org/10.1016/j.fuel.2017.09.057.
[22] G. Severa, K. Bethune, R. Rocheleau, S. Higgins, SO2 sorption by activated carbon supported ionic liquids under simulated atmospheric conditions, Chem. Eng. J. 265 (2015) 249–258, https://doi.org/10.1016/j.cej.2014.12.051.
[23] M.S. Raja Shahrom, A.R. Nordin, C.D. Wilfred, The improvement of activated carbon as CO2 adsorbent with supported amine functionalized ionic liquids, J. Environ. Chem. Eng. 7 (2019) 103319, , https://doi.org/10.1016/j.jece.2019.103319.
[24] K. Huang, F. Liu, J.P. Fan, S. Dai, Open and hierarchical carbon framework with ultralarge pore volume for efficient capture of carbon dioxide, ACS Appl. Mater. Interfaces 10 (2018) 36961–36968, https://doi.org/10.1021/acsami.8b12182.
[25] H.L. Peng, J.B. Zhang, J.Y. Zhang, F.Y. Zhong, P.K. Wu, K. Huang, J.P. Fan, F. Liu, Chitosan-derived mesoporous carbon with ultrahigh pore volume for amine impregnation and highly efficient CO2 capture, Chem. Eng. J. 359 (2019) 1159–1165, https://doi.org/10.1016/j.cej.2018.11.064.
[26] R. Duczinski, F. Bernard, M. Rojas, E. Duarte, V. Chaban, F.D. Vecchia, S. Menezes, S. Einloft, Waste derived MCMRH- supported IL for CO 2 /CH 4 separation, J. Nat. Gas Sci. Eng. 54 (2018) 54–64, https://doi.org/10.1016/j.jngse.2018.03.028.
[27] F. Liu, K. Huang, L. Jiang, Promoted adsorption of CO2 on amine-impregnated adsorbents by functionalized ionic liquids, AIChE J. 64 (2018) 3671–3680, https://doi.org/10.1002/aic.16333.
[28] F. Akti, Using of Modified SBA-15 Mesoporous Silica Materials for CO2 Capture, pp. 122–137. https://doi.org/10.4018/978-1-5225-3379-5.ch007.
[29] A. Andresova, J. Storch, M. Traïkia, Z. Wagner, M. Bendova, P. Husson, Branched and cyclic alkyl groups in imidazolium-based ionic liquids: molecular organization and physico-chemical properties, Fluid Phase Equilib. 371 (2014) 41–49, https://doi.org/10.1016/j.fluid.2014.03.004.
[30] H. Li, T. Zhang, S. Yuan, S. Tang, MCM-36 zeolites tailored with acidic ionic liquid to regulate adsorption properties of isobutane and 1-butene, Chin. J. Chem. Eng. 24 (2016) 1703–1711, https://doi.org/10.1016/j.cjche.2016.05.033.
[31] A. Ying, H. Hou, S. Liu, G. Chen, J. Yang, S. Xu, Ionic modified tbd supported on magnetic nanoparticles: a highly efficient and recoverable catalyst for organic transformations, ACS Sustain. Chem. Eng. 4 (2016) 625–632, https://doi.org/10.1021/acssuschemeng.5b01757.
[32] B. Karimi, M. Khorasani, F. Bakhshandeh Rostami, D. Elhamifar, H. Vali, Tungstate supported on periodic mesoporous organosilica with imidazolium framework as an efficient and recyclable catalyst for the selective oxidation of sulfides, Chempluschem 80 (2015) 990–999, https://doi.org/10.1002/cplu.201500010.
[33] F.J. Hernández-Fernández, A.P. de los Ríos, F. Tomás-Alonso, D. Gómez, G. Víllora, Improvement in the separation efficiency of transesterification reaction compounds by the use of supported ionic liquid membranes based on the dicyanamide anion, Desalination 244 (2009) 122–129, https://doi.org/10.1016/j.desal.2008.04.041.
[34] H. Srour, H. Rouault, C.C. Santini, Y. Chauvin, A silver and water free metathesis reaction: a route to ionic liquids, Green Chem. 15 (2013) 1341–1347, https://doi.org/10.1039/c3gc37034h.
[35] A.V. Perdikaki, O.C. Vangeli, G.N. Karanikolos, K.L. Stefanopoulos, K.G. Beltsios, P. Alexandridis, N.K. Kanellopoulos, G.E. Romanos, Ionic Liquid-modi Fi Ed Porous Materials for Gas Separation and Heterogeneous Catalysis, (2012).
[36] W.J. Koros, D.R. Paul, Design considerations for measurement of gas sorption in polymers by pressure decay, J. Polym. Sci. Polym. Phys. Ed. 14 (1976) 1903–1907, https://doi.org/10.1002/pol.1976.180141014.
[37] F.L. Bernard, B.B. Polesso, F.W. Cobalchini, V.V. Chaban, J.F. Do Nascimento, F. Dalla Vecchia, S. Einloft, Hybrid alkoxysilane-functionalized urethane-imide-Based poly(ionic liquids) as a new platform for carbon dioxide capture, Energy Fuels 31 (2017) 9840–9849, https://doi.org/10.1021/acs.energyfuels.7b02027.
[38] W. Span, R. Wagner, A new EOS for CO2 covering the fluid region from the triple point temperature to 1100K at pressures up to 800MPa.pDf, J. Phys. Chem. Ref. Data 25 (1996) 1509–1596, https://doi.org/10.1063/1.555991.
[39] M. Fernández Rojas, L. Pacheco Miranda, A. Martinez Ramirez, K. Pradilla Quintero, F. Bernard, S. Einloft, L.A. Carreño Díaz, New biocomposites based on castor oil polyurethane foams and ionic liquids for CO2capture, Fluid Phase Equilib. 452 (2017) 103–112, https://doi.org/10.1016/j.fluid.2017.08.026.
[40] A. Azimi, M. Mirzaei, Experimental evaluation and thermodynamic modeling of hydrate selectivity in separation of CO2 and CH4, Chem. Eng. Res. Des. 111 (2016) 262–268, https://doi.org/10.1016/j.cherd.2016.05.005.
[41] I.L. Soares, M.I.B. Tavares, A.L.B.B. e Silva, A.G.M. Feio, Carbon-13 solid state NMR techniques to evaluate the morphology of PP/TiO&sub&2&/sub& composites, Mater. Sci. Appl. Chem. 07 (2016) 20–25, https://doi.org/10.4236/msa.2016.71003.
[42] J.P. Korb, Nuclear magnetic relaxation of liquids in porous media, New J. Phys. 13 (2011), https://doi.org/10.1088/1367-2630/13/3/035016.
[43] K. Jin, T. Zhang, J. Ji, M. Zhang, Y. Zhang, S. Tang, Functionalization of MCM-22 by dual acidic ionic liquid and its paraffin absorption modulation properties, Ind. Eng. Chem. Res. 54 (2015) 164–170, https://doi.org/10.1021/ie504327t.
[44] V. Hiremath, A.H. Jadhav, H. Lee, S. Kwon, J.G. Seo, Highly reversible CO2 capture using amino acid functionalized ionic liquids immobilized on mesoporous silica, Chem. Eng. J. 287 (2016) 602–617, https://doi.org/10.1016/j.cej.2015.11.075.
[45] M. Thommes, K. Kaneko, A.V. Neimark, J.P. Olivier, F. Rodriguez-Reinoso, J. Rouquerol, K.S.W. Sing, Physisorption of gases, with special reference to the evaluation of surface area and pore size distribution (IUPAC Technical Report), Pure Appl. Chem. 87 (2015) 1051–1069, https://doi.org/10.1515/pac-2014-1117.
[46] P.K. Jal, M. Sudarshan, A. Saha, S. Patel, B.K. Mishra, Synthesis and characterization of nanosilica prepared by precipitation method, Colloids Surfaces A Physicochem, Int. J. Pavement Eng. Asph. Technol. 240 (2004) 173–178, https://doi.org/10.1016/j.colsurfa.2004.03.021.
[47] V. Dugas, Y. Chevalier, Chemical reactions in dense monolayers: in situ thermal cleavage of grafted esters for preparation of solid surfaces functionalized with carboxylic acids, Langmuir 27 (2011) 14188–14200, https://doi.org/10.1021/la2029438.
[48] S.A. Kulkarni, S.B. Ogale, K.P. Vijayamohanan, Tuning the hydrophobic properties of silica particles by surface silanization using mixed self-assembled monolayers, J. Colloid Interface Sci. 318 (2008) 372–379, https://doi.org/10.1016/j.jcis.2007.11.012.
[49] D. Valencia-Marquez, A. Flores-Tlacuahuac, R. Vasquez-Medrano, An optimization approach for CO2capture using ionic liquids, J. Clean. Prod. 168 (2017) 1652–1667, https://doi.org/10.1016/j.jclepro.2016.11.064.
[50] M. Xiao, H. Liu, H. Gao, W. Olson, Z. Liang, CO2 capture with hybrid absorbents of low viscosity imidazolium-based ionic liquids and amine, Appl. Energy 235 (2019) 311–319, https://doi.org/10.1016/j.apenergy.2018.10.103.
[51] T. Nonthanasin, A. Henni, C. Saiwan, Densities and low pressure solubilities of carbon dioxide in five promising ionic liquids, RSC Adv. 4 (2014) 7566–7578, https://doi.org/10.1039/c3ra46339g.
[52] M. Seferin, M.C. Corvo, J. Sardinha, J. Dupont, S. Einloft, G. Marin, S.C. Menezes, E.J. Cabrita, T. Casimiro, A rational approach to CO 2 capture by imidazolium ionic liquids: tuning CO 2 solubility by cation alkyl branching, ChemSusChem. 8 (2015) 1935–1946, https://doi.org/10.1002/cssc.201500104.
[53] L. Xue, E. Gurung, G. Tamas, Y.P. Koh, M. Shadeck, S.L. Simon, M. Maroncelli, E.L. Quitevis, Effect of alkyl chain branching on physicochemical properties of imidazolium-based ionic liquids, J. Chem. Eng. Data 61 (2016) 1078–1091, https://doi.org/10.1021/acs.jced.5b00658.
[54] F.K. Chong, V. Andiappan, D.K.S. Ng, D.C.Y. Foo, F.T. Eljack, M. Atilhan, N.G. Chemmangattuvalappil, Design of ionic liquid as carbon capture solvent for a bioenergy system: integration of bioenergy and carbon capture systems, ACS Sustain. Chem. Eng. 5 (2017) 5241–5252, https://doi.org/10.1021/acssuschemeng.7b00589.
[55] J. Ren, L. Wu, B.-G. Li, Preparation and CO $_2$ Sorption/Desorption of *N* -(3-Aminopropyl)Aminoethyl tributylphosphonium amino acid salt ionic liquids supported into porous silica particles, Ind. Eng. Chem. Res. 51 (2012) 7901–7909, https://doi.org/10.1021/ie2028415.
[56] F. Nkinahamira, T. Su, Y. Xie, G. Ma, H. Wang, J. Li, High pressure adsorption of CO 2 on MCM-41 grafted with quaternary ammonium ionic liquids, Chem. Eng. J. 326 (2017) 831–838, https://doi.org/10.1016/j.cej.2017.05.173.
[57] J. Ren, Z. Li, Y. Chen, Z. Yang, X. Lu, Supported ionic liquid sorbents for CO2capture from simulated flue-gas, Chin. J. Chem. Eng. 26 (2018) 2377–2384, https://doi.org/10.1016/j.cjche.2018.04.025.
[58] Y. Uehara, D. Karami, N. Mahinpey, CO2 adsorption using amino acid ionic liquid-impregnated mesoporous silica sorbents with different textural properties, Microporous Mesoporous Mater. 278 (2019) 378–386, https://doi.org/10.1016/j.micromeso.2019.01.011.
[59] W. Jeffrey Horne, M.S. Shannon, J.E. Bara, Correlating fractional free volume to CO2selectivity in [Rmim][Tf2N] ionic liquids, J. Chem. Thermodyn. 77 (2014) 190–196, https://doi.org/10.1016/j.jct.2014.03.012.
[60] Y. Ma, J. Gao, Y. Wang, J. Hu, P. Cui, Ionic liquid-based CO2 capture in power plants for low carbon emissions, Int. J. Greenh. Gas Control. 75 (2018) 134–139, https://doi.org/10.1016/j.ijggc.2018.05.025.
[61] C. Moya, M. Gonzalez-Miquel, F. Rodriguez, A. Soto, H. Rodriguez, J. Palomar, Non-ideal behavior of ionic liquid mixtures to enhance CO2capture, Fluid Phase Equilib. 450 (2017) 175–183, https://doi.org/10.1016/j.fluid.2017.07.014.
[62] J. Cheng, Y. Li, L. Hu, J. Liu, J. Zhou, K. Cen, CO 2 absorption and diffusion in ionic liquid [P 66614][Triz] modified molecular sieves SBA-15 with various pore lengths, Fuel Process. Technol. 172 (2018) 216–224, https://doi.org/10.1016/j.fuproc.

2017.12.022.
[63] J. Zhu, B. He, J. Huang, C. Li, T. Ren, Effect of immobilization methods and the pore structure on CO2separation performance in silica-supported ionic liquids, Microporous Mesoporous Mater. 260 (2018) 190–200, https://doi.org/10.1016/j.micromeso.2017.10.035.
[64] R. Santiago, J. Lemus, D. Moreno, C. Moya, M. Larriba, N. Alonso-Morales, M.A. Gilarranz, J.J. Rodríguez, J. Palomar, From kinetics to equilibrium control in CO2 capture columns using Encapsulated Ionic Liquids (ENILs), Chem. Eng. J. 348 (2018) 661–668, https://doi.org/10.1016/j.cej.2018.05.029.
[65] T. Zhao, X. Zhang, Z. Tu, Y. Wu, X. Hu, Low-viscous diamino protic ionic liquids with fluorine-substituted phenolic anions for improving CO2reversible capture, J. Mol. Liq. 268 (2018) 617–624, https://doi.org/10.1016/j.molliq.2018.07.096.
[66] B. Sasikumar, G. Arthanareeswaran, A.F. Ismail, Recent progress in ionic liquid membranes for gas separation, J. Mol. Liq. 266 (2018) 330–341, https://doi.org/10.1016/j.molliq.2018.06.081.
[67] Y.F. Liu, Q.Q. Xu, P. Cai, M.Y. Zhen, X.Y. Wang, J.Z. Yin, Effects of operating parameters and ionic liquid properties on fabrication of supported ionic liquid membranes based on mesoporous Γ-Al2O3 supports, J. Memb. Sci. 545 (2018) 176–184, https://doi.org/10.1016/j.memsci.2017.09.071.
[68] Z. Lei, C. Dai, W. Song, Adsorptive absorption: a preliminary experimental and modeling study on CO2solubility, Chem. Eng. Sci. 127 (2015) 260–268, https://doi.org/10.1021/jf5047464.
[69] D. Kodama, K. Sato, M. Watanabe, T. Sugawara, T. Makino, M. Kanakubo, Density, viscosity, and CO2Solubility in the ionic liquid mixtures of [bmim][PF6] and [bmim][TFSA] at 313.15 K, J. Chem. Eng. Data 63 (2018) 1036–1043, https://doi.org/10.1021/acs.jced.7b00786.
[70] P. Sharma, S. Do Park, K.T. Park, S.C. Nam, S.K. Jeong, Y. Il Yoon, I.H. Baek, Solubility of carbon dioxide in amine-functionalized ionic liquids: role of the anions, Chem. Eng. J. 193–194 (2012) 267–275, https://doi.org/10.1016/j.cej.2012.04.015.
[71] W.L. Theo, J.S. Lim, H. Hashim, A.A. Mustaffa, W.S. Ho, Review of pre-combustion capture and ionic liquid in carbon capture and storage, Appl. Energy 183 (2016) 1633–1663, https://doi.org/10.1016/j.apenergy.2016.09.103.
[72] M. Klähn, A. Seduraman, What determines CO < inf > 2 < /inf > solubility in ionic liquids? A molecular simulation study, J. Phys. Chem. B 119 (2015) 10066–10078, https://doi.org/10.1021/acs.jpcb.5b03674.
[73] M. Zoubeik, A. Henni, Experimental and thermodynamic study of CO2 solubility in promising [TF2N and DCN] ionic liquids, Fluid Phase Equilib. 376 (2014) 22–30, https://doi.org/10.1016/j.fluid.2014.05.021.
[74] L.C. Tome, I.M. Marrucho, Ionic liquid-based materials: a platform to design engineered CO2 separation membranes, Chem. Soc. Rev. 45 (2016) 2785–2824, https://doi.org/10.1039/C5CS00510H.
[75] M. Ramdin, T.W. De Loos, T.J.H. Vlugt, State-of-the-art of CO \n 2 capture with ionic liquids, Ind. Eng. Chem. Res. 51 (2012) 8149–8177, https://doi.org/10.1021/ie3003705.